

Jefferson Lab

System and Infrastructure Design Review
May 7-9, 2008

Hall D Trigger Simulation

The GlueX Collaboration
E. Chudakov and A. Somov

April 30, 2008

Contents

1	Introduction	2
2	Photon Beam and Photoproduction Rate	3
3	Simulation of Photoproduction	6
4	Trigger Simulation	10
4.1	Trigger Algorithm	11
4.2	Event Size	13
4.3	Outlook	15
5	Conclusion	23

1 Introduction

The goal of the experiment is the search for hybrid/exotic mesons produced by a photon beam on a liquid hydrogen target. These mesons would decay to final states containing charged pions and photons. The charged particles are detected by the drift chambers. They give signals in one of the calorimeters and may hit the forward TOF scintillators. The charged particle momentum will not be evaluated in the first-level trigger. The photons are detected with the calorimeters and their energy will be evaluated at this stage.

The first-level trigger can use signals from:

- the forward calorimeter (FCAL);
- the barrel calorimeter (BCAL);
- the forward time-of-flight plastic scintillator detector (TOF);
- the plastic scintillator start-counter;
- the photon beam tagger plastic scintillator counter.

Final states of the hybrid meson decays are not expected to differ strongly from the ordinary photoproduction processes, which could have provided a signature for their separation from the background on the trigger level. Therefore, the experiment needs a soft trigger which accepts nearly all hadronic events produced by the beam photons in a certain energy range. At this stage, only the events outside of the required energy range are considered background.

Purely electromagnetic interactions of the beam in the target, as such pair production, although strongly suppressed in the spectrometer by the solenoidal magnetic field and the detector arrangement, can give signals in the individual detectors. They can either fire the trigger, or pile up in low energy hadronic events, thus faking larger energies and increasing the background rate.

2 Photon Beam and Photoproduction Rate

Photons are produced by the 12-GeV electron beam on a diamond crystal via both incoherent and coherent Bremsstrahlung processes. The spectrum of the coherent photons is concentrated in several peaks of different strengths, whose positions as well as the degree of the photon's linear polarization depends on the crystal's orientation. The coherent component is relatively stronger at smaller Bremsstrahlung angles. The beam parameters have been optimized for GlueX [1]:

- The diamond crystal is 20 μm thick;
- The collimator of a 3.4 mm diameter is positioned at a 76 m distance from the crystal;
- The main coherent Bremsstrahlung peak is located at $\sim 8.4 - 9.0$ GeV;

The experiment should be able to run with the photon flux of 100 MHz in the main peak $E \sim 8.4 - 9.0$ GeV. This intensity can be provided by a $\sim 2 \mu\text{A}$ electron beam. At the initial stage, the experiment will run at a beam intensity ten times lower.

An ideal trigger would select only the events in the range of 8.4-9.0 GeV.

The calculated beam spectra above the photoproduction threshold are shown in Fig. 1(a). In this range of 0.15-12 GeV, the tagger rate is 10 GHz. Because of the collimation, the beam rate is about 7 times lower at 1.5 GHz. In the useful range of 8.4-9.0 GeV the tagger rate of 250 MHz is 2.5 times higher than the beam rate.

The tagger could provide an efficient way to select the energy range of the accepted events. However, at the high beam intensity the tagger rate is too high, since about 50% of accelerator pulses arriving at 500 MHz will provide at least one hit in the useful range of the tagger.

The hadronic photoproduction rate on a 30 cm long liquid hydrogen target was calculated using the full photoproduction cross section, tabulated by the PDG group [2] (see Fig. 1(b)).

The expected rates are summarized in Table 1. The full photoproduction rate of 360 kHz is dominated by the low energy part. The rate in the coherent peak is 16 kHz.

Should the first-level trigger select only events for beam energies above 2 GeV, it would reduce the trigger rate to 100 kHz.

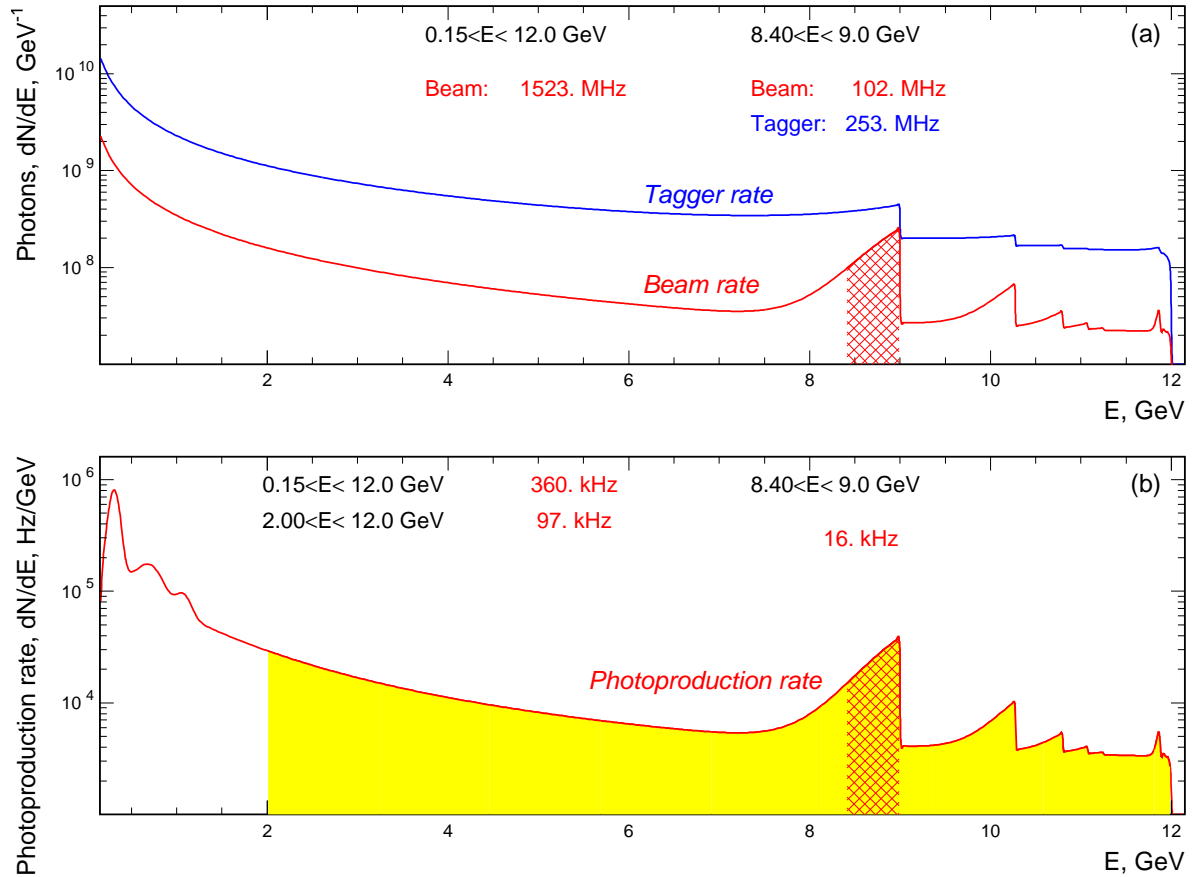


Figure 1: The top figure (a) shows the energy spectra for the photons before and after the collimator. The former spectrum (in blue) demonstrates the expected rate on the beam tagger, while the latter one (in red) is the spectrum of the beam seen by the experiment. The collimated beam has the coherent peak enhanced relatively to the incoherent contribution. The useful beam energy area of 8.4-9.0 GeV is shaded. The bottom figure (b) shows the hadronic photoproduction rate. The useful area is shaded. A broader shaded area, of 2.0-12. GeV indicates the energy range which can likely be identified by the first-level trigger.

Rates	Energy range, GeV		
	0.15 - 12.	2.0 - 12.	8.4 - 9.0
Tagger	10 GHz	4.0 GHz	250 MHz
Beam	1.5 GHz	670 MHz	100 MHz
Photoproduction	360 kHz	100 kHz	16 kHz

Table 1: The expected rates at the high luminosity running, in various energy intervals. The bottom row shows the hadronic rate.

3 Simulation of Photoproduction

The photoproduction processes have been simulated using the following scheme:

- The energy spectrum of the interacting photons was calculated using the beam energy spectrum and the total photoproduction cross section (see Fig. 1(b));
- At the beam energies below 3 GeV an admixture of several dominant reactions was simulated, their relative differential cross sections were taken from the existing data;
- Above 3 GeV the PYTHIA generator [3] was used, slightly adapted for low energies.

PYTHIA was designed and tuned by the authors for much higher energies. Special efforts were taken by the HERMES collaboration to adapt it to the HERA electron energy of ~ 30 GeV. We slightly adapted the version from HERMES to the energies as low as 3 GeV, and compared the PYTHIA results with some experimental data. At 9 GeV PYTHIA underestimates the total photoproduction cross section, providing $\sim 80 \mu\text{b}$ instead of $\sim 120 \mu\text{b}$. However, the partial cross sections from PYTHIA, scaled up by a factor $120/80=1.5$ are in a reasonable agreement with the data (see Table 2 and also [4]).

process $\gamma p \rightarrow$	via	Experiment		PYTHIA	
		$E_\gamma, \text{ GeV}$	$\sigma, \mu\text{b}$	$E_\gamma, \text{ GeV}$	$\sigma, \mu\text{b}$
1 prong		9.3	8.5 ± 1.0	9.0	6.2
3 prong		9.3	64.4 ± 1.5	9.0	59.0
5 prong		9.3	34.2 ± 0.9	9.0	44.0
7 prong		9.3	6.8 ± 0.3	9.0	8.3
$p\pi^+\pi^-$	$p\rho^\circ$	9.3	14.7 ± 0.6	9.0	14.5
		9.3	13.5 ± 0.5	9.0	13.0
$p\pi^+\pi^-\pi^\circ$	$p\rho$	9.3	7.5 ± 0.8	9.0	7.0
		9.3	1.9 ± 0.3	9.0	1.4
$p2\pi^+2\pi^-$		9.3	4.1 ± 0.2	9.0	3.7

Table 2: Comparison of the partial cross sections provided by PYTHIA with the data. The PYTHIA results were scaled by a factor of 1.5.

At the energies below 1 GeV the dominant process is the single pion production, which is not simulated well by PYTHIA. On the other hand, these processes have been well parametrized in the framework of MAID and SAID systems [5]. At energies below 3 GeV only about 10 processes with small multiplicities comprise more than 95% of the total cross section. The differential cross sections for these processes have been well measured. Above 3 GeV more reactions with higher multiplicities and more complex differential cross sections step in. Therefore, we applied the hybrid approach, using

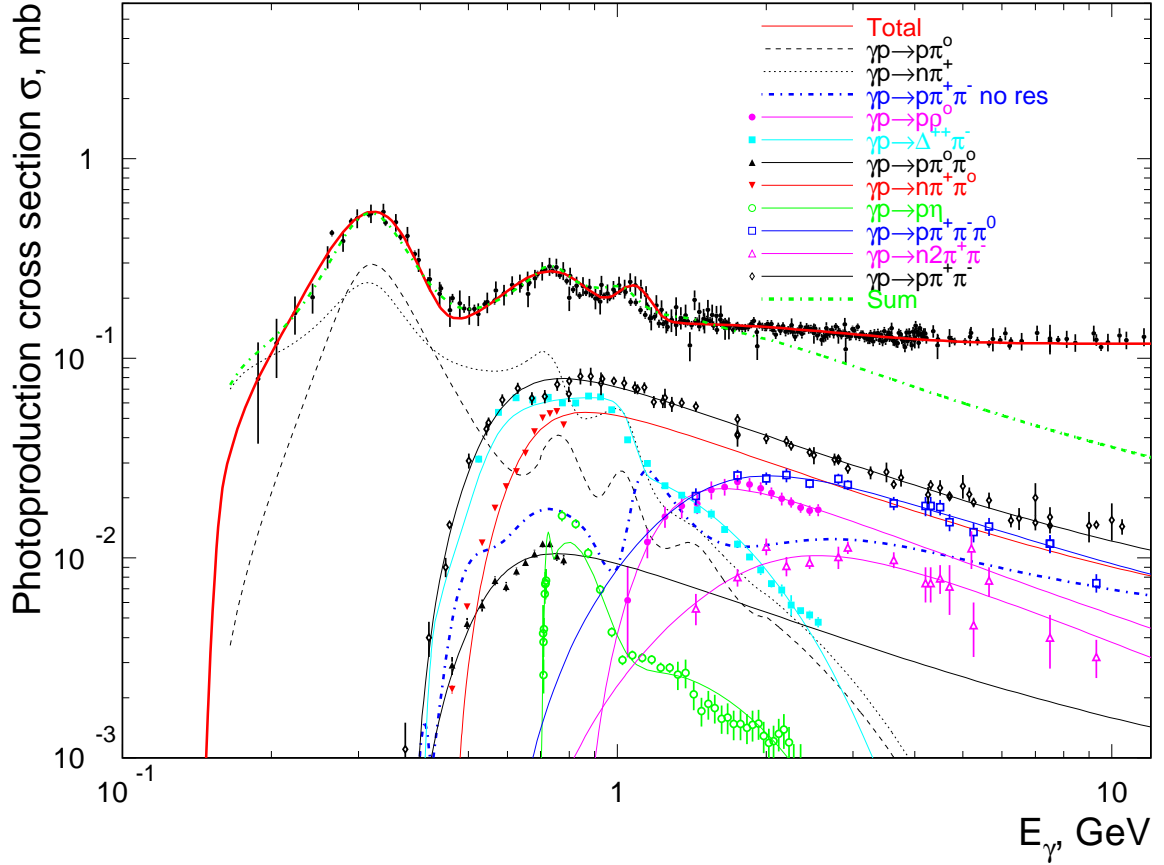


Figure 2: The total photoproduction cross section (the red solid curve) and the partial cross sections for the reactions used at the energies below 3 GeV. The sum of all these partial cross sections (the green dotted curve) matches the total cross section very well, below 2 GeV. At 3 GeV the sum is about 30% smaller than the total cross section. For the simulation, all the partial cross sections were normalized to keep their sum equal to the total cross section.

#	Process	Experimental data		Simulation		Comment
		Range, GeV	$d^n\sigma/dp^n$	Rate	$d^n\sigma/dp^n$	
1	$p\pi^\circ$	0.15 - 2.00	$\frac{d\sigma}{d(\cos\theta_{CM})}$	SAID	SAID	
2	$n\pi^+$	0.15 - 2.00	$\frac{d\sigma}{d(\cos\theta_{CM})}$	SAID	SAID	
3	$p\pi^+\pi^-$	0.40 -12.00	$d\sigma/dt$		total, used to extract (6)	
4	$p\rho^\circ$	1.00 - 2.50	$d\sigma/dt$	exp	exp	$\rho^\circ \rightarrow \pi^+\pi^- : \sin\theta_{CM}$
5	$\Delta^{++}\pi^-$	0.40 - 3.00	$d\sigma/dt$	exp	exp	$\Delta^{++} \rightarrow p\pi^+$
6	$p\pi^+\pi^-$	0.40 -12.00	$d\sigma/dt$	(3)-(4)-(5) non-resonant, by subtraction		
7	$p\pi^\circ\pi^\circ$	0.40 -0.80	$d\sigma/dt$	exp	phase space	
8	$n\pi^+\pi^\circ$	0.40 -0.80	$d\sigma/dt$	exp	phase space	
9	$p\eta$	0.70 -2.50	$\frac{d\sigma}{d(\cos\theta_{CM})}$	exp	exp	
10	$p\pi^+\pi^-\pi^\circ$	1.50 -10.00	$d\sigma/dt$	exp	phase space	
11	$n\pi^+\pi^+\pi^-$	1.50 -10.00	$d\sigma/dt$	exp	phase space	

Table 3: The reactions used to simulate the low energy background. The columns 4 and 6 show the source of the differential cross sections. Typically, the t -distributions have been measured. If the simulation was based on experimental data, the columns 5 and 6 indicate it with a note “exp”. For the multi-meson states the uniform phase space distribution was used. The reaction (3) was not simulated, but used to extract the non-resonant contribution (6). The data were taken from the compilation [6] and from the HEPDATA reaction data base [7].

PYTHIA above 3 GeV and a compilation of the data on the dominant reactions below 3 GeV. These reactions are summarized in Table 3.

The total and the partial cross sections are presented in Fig. 2. The reaction admixture describes the total cross section very well below 2 GeV. At 3 GeV the sum is about 30% smaller than the total cross section. For the simulation, all the partial cross sections were normalized to keep their sum equal to the total cross section. Still, the discrepancy indicates that other processes, presumably with higher multiplicity step in between 2 and 3 GeV. This is demonstrated in Fig. 3.

The energy dependence of the π^+ multiplicity is relatively smooth, while the π^- and π° multiplicities have a dip just below 3 GeV. Because of this, about 6% of all simulated background events have π^- and π° multiplicities underestimated by $\sim 10\%$. The total event energy is not affected. We expect that this effect will not distort the estimate of the trigger rejection power by more than 1-2%.

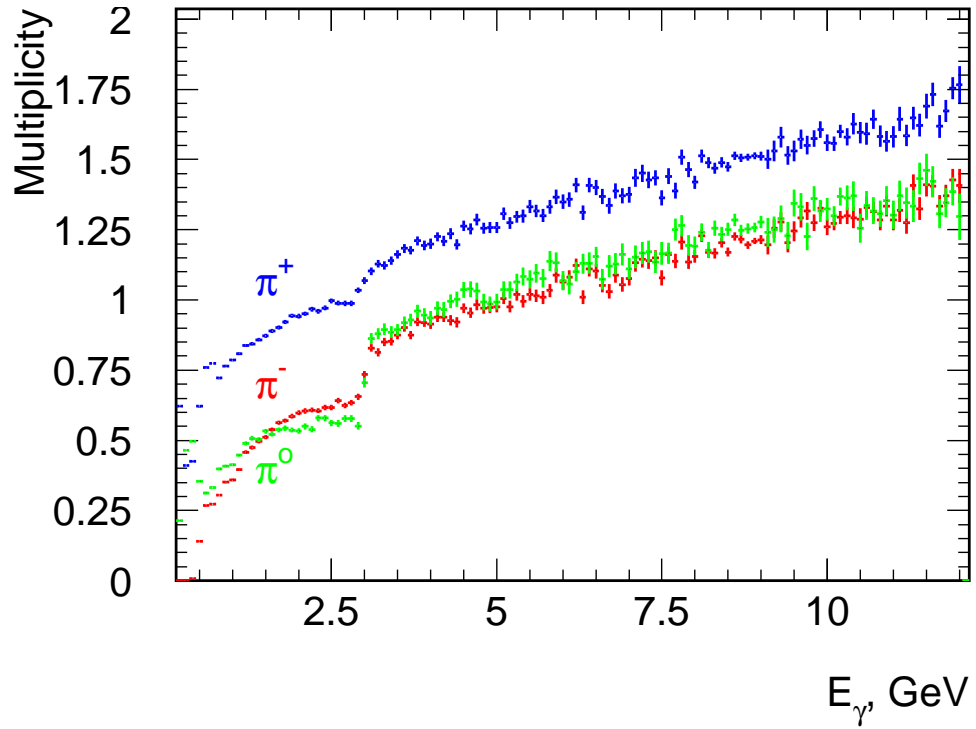


Figure 3: The average simulated multiplicities for pions. The dip at 2-3 GeV is an artefact of applying two different models for production below and above 3 GeV. Possible implications for the current studies are discussed in the text.

4 Trigger Simulation

The GlueX detector will start taking data at a luminosity corresponding to about 10^7 photons per second in the photon-beam energy range of $8.4 \leq E_\gamma \leq 9.0$ GeV. Later, the luminosity will be increased by an order of magnitude to 10^8 photons per second. When running at low luminosity, the Level-1 trigger has to reduce the rate from electromagnetic and hadronic interactions seen by the GlueX detector to a level acceptable by a data acquisition for writing events directly to tape, about 20 kHz. For high luminosity runs, events accepted by the Level-1 trigger will be sent to the third level trigger at the rate which should not exceed 200 kHz. The Level-3 trigger will perform an event reconstruction on a PC farm allowing to further reduce low-energy photon interactions and providing an additional rate reduction of about factor of 10. After the Level-3 trigger events will be recorded to tape.

In this section we investigate the feasibility of achieving a sufficient rate reduction on the example of operating the Level-1 trigger at high luminosity, 10^8 photons per second. In order to determine the trigger algorithm we perform a full GEANT [8] detector simulation. The reconstruction of energy deposition in the calorimeters is based on a Monte Carlo (MC) simulation calibrated according to results from test beam and cosmic data [9]. We consider two sources of backgrounds:

- electromagnetic interactions of beam photons
- photoproduction of hadrons at low photon-beam energies, $E_\gamma \leq 8$ GeV

The electromagnetic background is modeled for Bremsstrahlung photons in the energy range of $1.1 \text{ MeV} \leq E_\gamma \leq 12.0 \text{ GeV}$ ¹. The intensity of the photon beam is about 3×10^9 . The electromagnetic interactions in this energy range originate mainly from a e^+e^- pair production and Compton scattering processes; the cross section of the later process dominates for $E_\gamma \leq 0.2$ GeV. The interaction rate of the beam photons in the target region constitute about 50 MHz and 140 MHz for the pair production and Compton scattering, respectively. As there is no vacuum beam pipe starting from the target region, interactions of the beam photons occur along the entire detector range up to the position of FCAL, resulting in the total rates of about 91 MHz and 208 MHz for $\gamma p \rightarrow e^+e^-$ and 208 MHz for $\gamma e \rightarrow \gamma e$. To reduce photon conversion and consequently occupancies in the FCAL and TOF, especially in the regions close to the beam line, we consider to use a He-bag after the FDC.

The polar angle and energy of $e^+(e^-)$ produced in $\gamma p \rightarrow e^+e^-$ reaction is shown in Fig. 4. The polar angle is defined as the angle between the beam direction and the momentum of $e^+(e^-)$. The corresponding distributions for γ and e^- originating from $\gamma e \rightarrow \gamma e$ process is presented in Fig. 5. As can be seen from these plots, most e^+ (e^-) tracks produced from the gamma conversion go to the forward direction, i.e., they will be mainly seen by the 'forward' detectors, TOF and FCAL. At the same time, the low

¹The low energy of photons is set close to the threshold of a e^+e^- pair production. For hadronic photoproduction the energy spectrum starts at $E_\gamma = 0.15$ GeV, the production threshold of $p\pi$.

energy photons and electrons from Compton scattering are distributed over larger polar angles. The rates for these two processes for the different detector components are listed in Table 4. The rate is calculated by counting the number of events with at least one hit in the corresponding subdetector.

	Start Counter	FCAL	BCAL	TOF
Rate (MHz)	2.5	5.9	0.4	41.9

Table 4: Subdetector rates for electromagnetic background. The thresholds to define a hit in the FCAL and BCAL are set to 30 MeV.

The generation of hadronic interactions from photoproduction has been explained in Section 3. The hadronic background is defined as events produced at low beam energies, $E_\gamma < 8.0$ GeV. We study the trigger rate using hadronic events produced in the whole energy range of photons ($0.15 \text{ GeV} \leq E_\gamma$) while a trigger probability is estimated for interactions of interest if the beam energy satisfies $E_\gamma \geq 8.0$ GeV. We refer to events with $E_\gamma \geq 8.0$ GeV as hadronic 'signal' events. As has been discussed in Section 1, the topology of events generated with PYTHIA for a large photon-beam energy is very similar to that predicted for exotic mesons. The trigger efficiency is checked by applying the trigger algorithm to signal MC events generated for some 'typical' exotic decay channels, results will be presented during the review.

To account for the hardware performance, we conservatively assume a trigger integration time interval of 100 ns for all subdetectors. In reality, this gate will be different for the various detector components used in the trigger. We expect that BCAL would have the largest pulse length with the main contribution coming from electronics (about 40-50 ns) and light propagation in 4-meter-long scintillator fibers (~ 25 ns). The JLAB accelerator facility provides an electron beam with a bunch rate of 500 MHz. Electrons in each bunch produce on average six bremsstrahlung beam photons which pass the target region. The beam photons result in about 0.4 electromagnetic interactions per bunch. Multiple electromagnetic interactions, on average 20, will appear during 100 ns interval. We model pileup events by superimposing electromagnetic interactions in this time window on each event. The particles produced in the electromagnetic interactions are subsequently added to that from the standard generation mechanism. We generate MC events for signal and backgrounds corresponding to the 100 ns time interval and use these events to study the trigger probability and rejection.

In the next section we describe a simple trigger algorithm which is based on measurements of the number of hits in the start counter and energy deposition in the FCAL and BCAL.

4.1 Trigger Algorithm

To show the capabilities of the Level-1 trigger design, a simple trigger algorithm has been developed, which is able to provide sufficient background rejection and, at the same time,

keep the trigger efficiency for decays of interest at a level close to 100%. The algorithm is based on conditional thresholds applied to the hit multiplicity in the start counter (SC) and the energy depositions in the FCAL and BCAL. To determine these thresholds we study correlations among the number of hits in the SC and energies released in the calorimeters for background and signal events.

We classify all events into two categories: events with and without hits in the start counter, and apply different trigger thresholds for these two categories. Hit multiplicities in the start counter for electromagnetic and hadronic backgrounds, as well as for the signal events are shown in Fig. 6. As expected, a major fraction of electromagnetic background events, about 78.2%, produce no hits in the start counter. In contrast, almost all signal events (98.6%) have a track(s) within the acceptance of the start counter (the polar-angle acceptance lies between 3.0° and 134°) producing at least one hit. Note that in γp interactions there must be at least one charged track in the final state. The energy deposition in the FCAL and BCAL for signal and background events with no hits in the SC is presented in Fig. 7. The average energies deposited in the calorimeters are listed in Table 5. Fig. 7 shows that the electromagnetic background releases relatively small energy in the BCAL. Electromagnetic and hadronic backgrounds are rejected requiring the BCAL energy in the event to be larger than 0.2 GeV and the total energy in the BCAL and FCAL to be greater than 2 GeV. We also apply a threshold on the FCAL energy $E_{\text{FCAL}} > 30$ MeV. After these requirements, the rate for electromagnetic (hadronic) background is significantly reduced from 7.82 MHz (12 kHz) to 4 kHz (0.2 kHz). The contribution to the trigger rate from electromagnetic background with no hits in the start counter is negligible. The rates are listed in Table 6. The fraction of hadronic signal events with no hits in the start counter is about 1.4% of the total signal events. The thresholds on the energy deposition have to be further optimized using MC simulation for particular exotic decay channels.

Process type	E_{BCAL} GeV		E_{FCAL} GeV	
	$N_{\text{SC}} = 0$	$N_{\text{SC}} > 0$	$N_{\text{SC}} = 0$	$N_{\text{SC}} > 0$
Electromagnetic	0.014	0.105	0.124	0.199
Hadronic $E_\gamma < 8$ GeV	0.277	0.578	0.212	0.304
Hadronic $E_\gamma > 8$ GeV	1.168	1.978	2.451	2.074

Table 5: Average energy deposition in the BCAL and FCAL for backgrounds and hadronic events with the beam-photon energy $E_\gamma > 8$ GeV. Energies are calculated for events with no hits ($N_{\text{SC}} = 0$) and with at least one hit ($N_{\text{SC}} > 0$) in the start counter.

Much larger contributions to the trigger rate come from events which have hits in the start counter. The energy distribution in the FCAL and BCAL for signal and background events with at least one hit in the SC is shown in Fig. 8. The electromagnetic and

hadronic backgrounds can be substantially reduced by applying an asymmetric threshold on the energy deposition in both calorimeters, i.e. we reject low-energy events requiring $E_{\text{BCAL}} + E_{\text{FCAL}} \times 0.5/2.0 \geq 2.0$. This requirement is shown as a solid diagonal curve in Fig. 8. The resulting trigger rates and probabilities of accepting hadronic events with $E_\gamma > 8$ GeV for various thresholds are listed in Table 6. As can be seen, the total electromagnetic and hadronic rate does not exceed 150 KHz which is below our trigger requirements of 200 KHz. The probability of accepting hadronic events with $E_\gamma > 8.0$ GeV is about 93%. The energy spectra of beam photons for all hadronic interactions and those accepted by the Level-1 trigger are presented in Fig. 9.

Finally, we consider a trigger algorithm which is only based on the BCAL and FCAL energies only. This implies that the start counter information is no longer used in the Level-1 trigger. We apply the following threshold: $E_{\text{BCAL}} > 0.03$ GeV, $E_{\text{FCAL}} > 0.03$ GeV, and $E_{\text{BCAL}} + E_{\text{FCAL}} \times 0.5/2.0 \geq 2.0$. These thresholds are similar to that used for events with $N_{\text{SC}} > 0$ described in the previous paragraph. We found that a trigger rate increases by only about 21 kHz compared to that when the hit information from the start counter is used, due to the additional contribution from electromagnetic background. The overall trigger rate constitutes ~ 170 kHz, which is still below 200 kHz.

In the next section we will estimate a size of events accepted by the Level-1 trigger. Possibilities for the further improvement of the trigger algorithm will be discussed in Section 4.3.

4.2 Event Size

We estimate the size of events which are accepted by the Level-1 trigger by counting the number of bytes which are sent from the electronics boards, F1TDC, FADC-125, and FADC-250. We assume a 100 ns readout time interval for most detector components except for the FDC and CDC, where the time intervals are chosen to be larger due to the drift time measurement. We require the readout times of 300 ns and 1 μs for the FDC and CDC, respectively. The detector occupancies are studied using MC events generated for signal and backgrounds. In the MC simulation we model pile-up events for electromagnetic background in a 100 ns time window, as has been described in Section 4. The detector occupancies are listed in Table 7. To estimate the number of hits in the FDC in a 300 ns time interval, we add to the FDC hit multiplicities simulated for the 100 ns interval an average number of hits produced by the electromagnetic background in a 200 ns time window. The CDC occupancy is calculated in a similar way.

The event sizes for the signal and backgrounds are obtained by multiplying the average detector occupancies by the number of bytes per hit needed to code measured time and amplitude. The F1TDC's and FADC's use a 32-bit word to send the hit time or amplitude. A data flow from each type of electronics board is presented in Tables 8 and 9. The sizes of events accepted by the Level-1 trigger for electromagnetic background, hadronic background, and hadronic signal events are found to be 14.8 kB, 15.0 kB, and 16.9 kB, respectively. An average event size is calculated by weighting individual contributions from the signal and backgrounds according to their relative trigger rates,

$N_{\text{SC}} = 0$. Trigger Rate (kHz)				
	No cuts	$E_{\text{BCAL}} > 0.2 \text{ GeV}$	$E_{\text{FCAL}} > 0.03 \text{ GeV}$	$E_{\text{FCAL+BCAL}}$
Electromagnetic	7816	23.9	15.9	4.00
Hadronic $E_\gamma < 8.0 \text{ GeV}$	12.7	8.03	4.03	0.23
Hadronic $E_\gamma > 8.0 \text{ GeV}$	0.43	0.18	0.18	0.17
Total				4.4
$N_{\text{SC}} = 0$. Trigger Probability (%)				
Hadronic $E_\gamma > 8.0 \text{ GeV}$	100.0	41.7	41.7	38.9
$N_{\text{SC}} > 0$. Trigger Rate (kHz)				
	No cuts	$E_{\text{BCAL}} > 30 \text{ MeV}$	$E_{\text{FCAL}} > 30 \text{ MeV}$	$E_{\text{FCAL+BCAL}}$
Electromagnetic	2184	317	214	60.5
Hadronic $E_\gamma < 8.0 \text{ GeV}$	314.2	268.5	164.9	54.6
Hadronic $E_\gamma > 8.0 \text{ GeV}$	32.7	30.9	30.8	30.2
Total				145.3
$N_{\text{SC}} > 0$. Trigger Probability (%)				
Hadronic $E_\gamma > 8.0 \text{ GeV}$	100.0	94.5	94.1	92.4

Table 6: The trigger rates and probabilities of accepting hadronic ‘signal’ events calculated for various thresholds sequentially applied to the energy depositions in the FCAL and BCAL. $E_{\text{FCAL+BCAL}}$ denotes the energy-dependent threshold described in the text. The rates and probabilities are calculated for two event categories: events without ($N_{\text{SC}} = 0$) and with ($N_{\text{SC}} = 0$) hits in the start counter. Note, the fraction of hadronic signal events with $N_{\text{SC}} = 0$ is small, 1.4% of the total number of signal events.

see Table 6. The average event size is found to be 15.3 kB.

4.3 Outlook

We developed a simple Level-1 trigger algorithm which is able to reduce the rate of electromagnetic and hadronic interaction to a level below 200 kHz when operating at high luminosity (10^8 photons per second) and provide the trigger probability for decays of interest of about 92%. The algorithm is based on thresholds applied to the energy depositions in the FCAL and BCAL and the hit multiplicity in the start counter. Though the rate reduction achieved by the trigger is sufficient for operating the GlueX detector at both high and low luminosities, the trigger algorithm could be further improved in the future in terms of optimizing the trigger efficiency and background rejection. The sources of potential improvements are:

- study event topologies for signal and background events; require energy releases in different FCAL regions
- develop more sophisticated algorithm rather than applying thresholds on energy and hit distributions
- integrate the hit information of the TOF into the trigger
- use Tagger information

Detector	Electromagnetic	Hadronic $E_\gamma < 8.0$ GeV	Hadronic $E_\gamma > 8.0$ GeV
Start Counter	2.7	3.2	4.0
BCAL	61.9	83.6	112.2
FCAL	11.5	8.9	17.9
TOF	32.3	28.7	38.8
CDC	49.9	62.7	70.5
FDC anode	28.9	28.3	46.9
FDC cathode	275.8	269.9	444.6

Table 7: Hit multiplicities in various subdetectors for events accepted by the Level-1 trigger. The hit multiplicities correspond to a 100 ns readout time interval. Thresholds on the cell energies in the BCAL and FCAL are set to 2.6 MeV and 0.2 GeV, respectively.

F1TDC			
Detector	N_{EM}	$N_{\text{Had}} E_\gamma < 8.0 \text{ GeV}$	$N_{\text{Had}} E_\gamma > 8.0 \text{ GeV}$
Start Counter	3	3	4
BCAL	62	84	112
TOF	32	29	39
FDC anode	87	86	105
Tagger	25		
Total hits	209	227	285
bytes/hit = 4 (32 bits)			
Address: 137 boards \times 4 bytes (event header) = 548			
Total bytes	1384	1456	1688
FADC-125			
FDC cathode	828	822	997
CDC	500	513	521
Total hits	1328	1335	1518
bytes/hit: 4 Integral + 4 time = 8			
Address: 188 boards \times 4 bytes (event header) = 752			
Total bytes	11376	11432	12896

Table 8: Average number of hits N for background and signal events accepted by the Level-1 trigger and the number of bytes read out from all F1TDC and FADC-125 boards.

FADC-250			
Detector	N_{EM}	$N_{Had} E_\gamma < 8.0 \text{ GeV}$	$N_{Had} E_\gamma > 8.0 \text{ GeV}$
Start Counter	3	3	4
BCAL	62	84	112
FCAL	12	9	18
TOF	32	29	39
Tagger	25		
Total hits	134	150	198
bytes/hit: 4 Integral (all detectors); 4 time (FCAL)			
Address: 374 boards \times 4 bytes (event header) = 1496			
Total bytes	2080	2132	2360
Total event size, bytes	14840	15020	16944

Table 9: Average number of hits N for background and signal events accepted by the Level-1 trigger and the number of bytes read out from all FADC-250 boards.

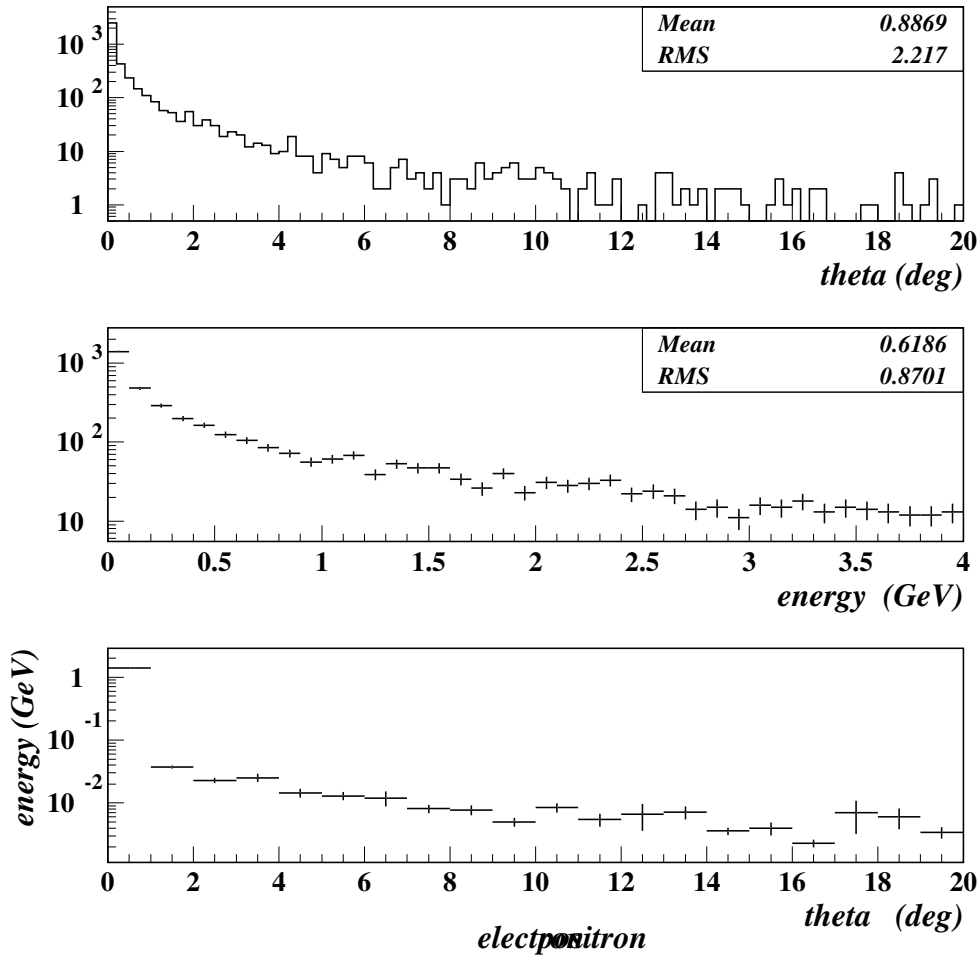


Figure 4: The distributions of polar angle (top), energy (middle), and energy versus polar angle (bottom) distributions for e^+ and e^- produced in $\gamma p \rightarrow e^+ e^-$ interactions on target.

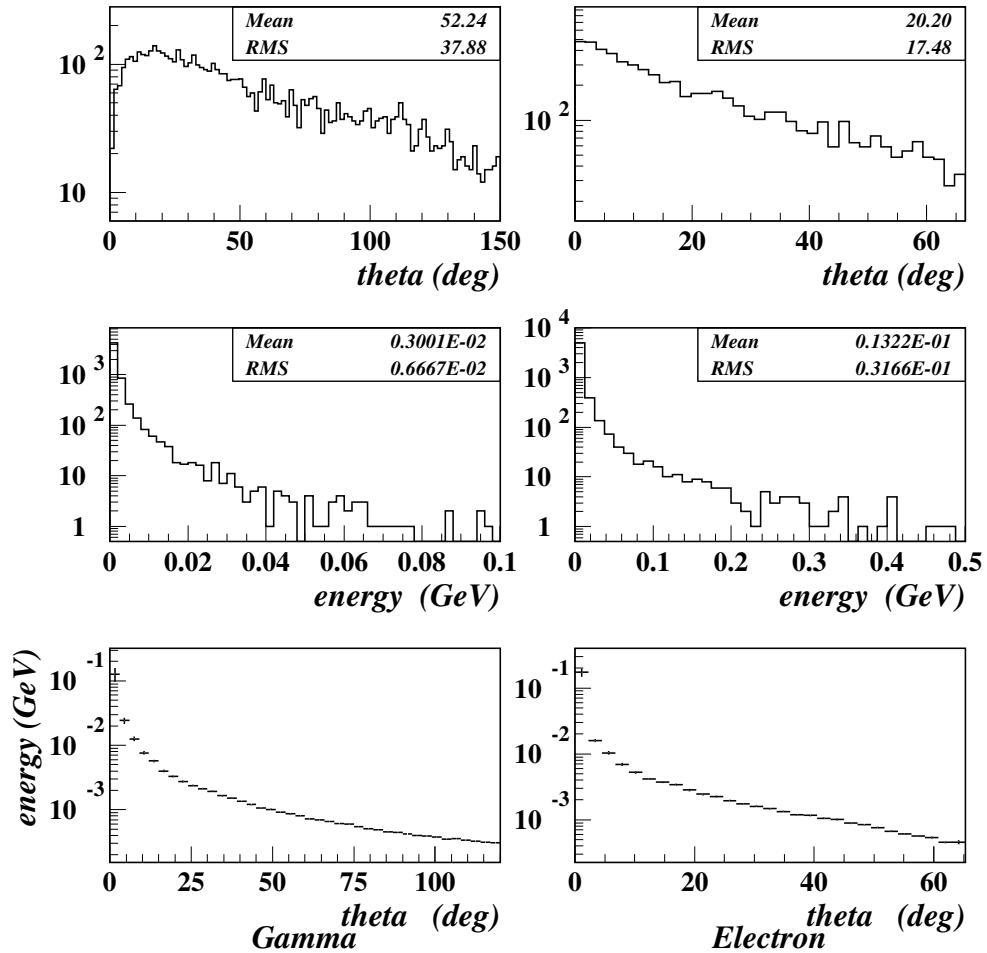


Figure 5: The polar angle (top), energy (middle), and energy versus polar angle (bottom) of photons (left column) and electrons (right column) for Compton scattering of the beam photons on target.

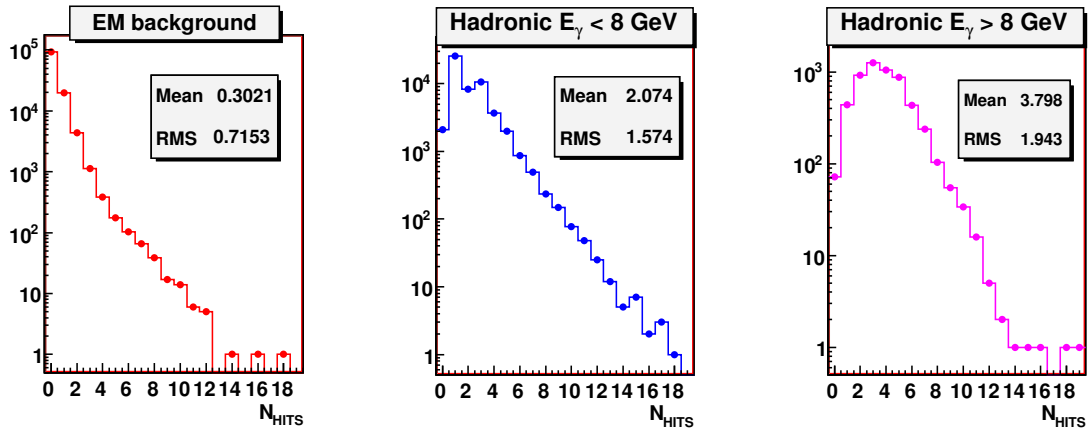


Figure 6: The hit multiplicities in the start counter for electromagnetic background (left), hadronic background (middle), and hadronic event with the beam energy in the signal region (right).

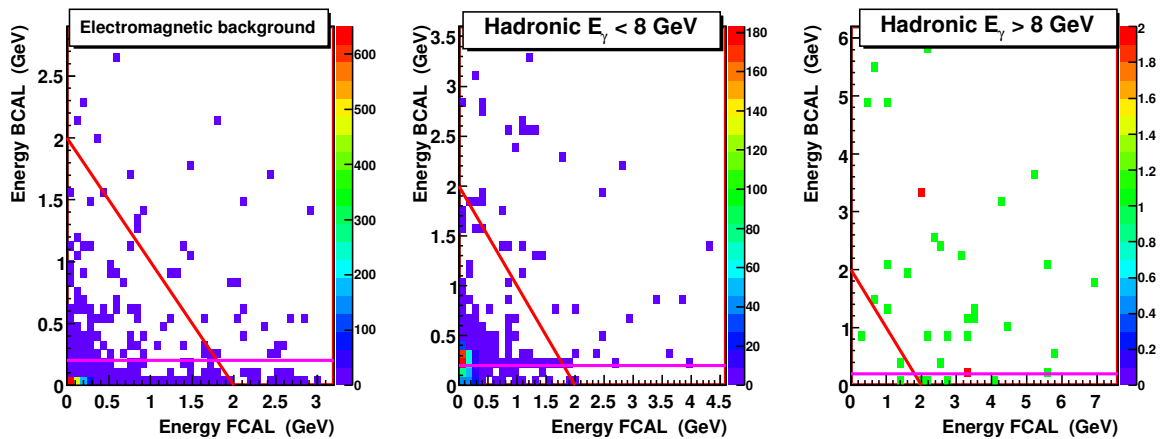


Figure 7: BCAL energy versus FCAL energy for events with no hits in the start counter for electromagnetic background (left), hadronic background (middle), and signal events (right). The solid curve represents the threshold applied in the analysis.

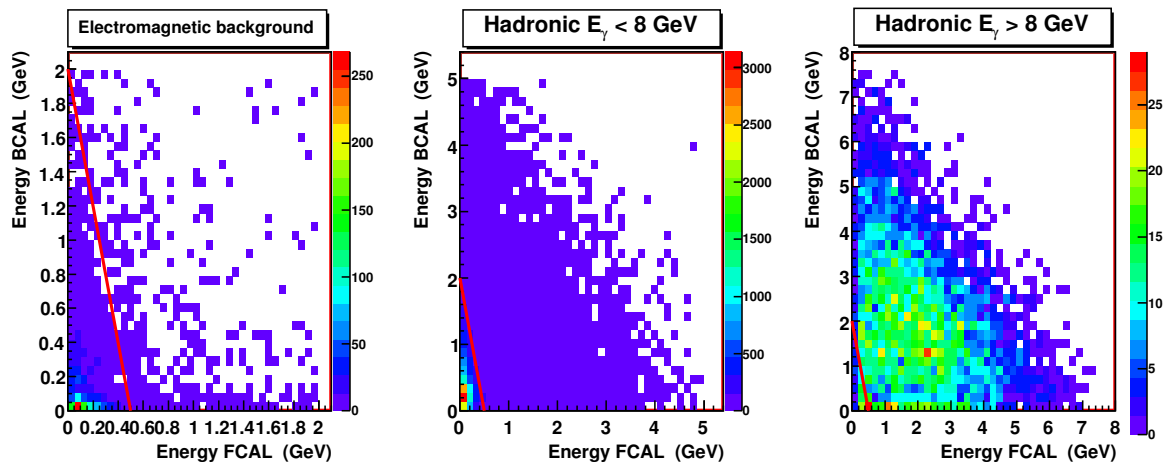


Figure 8: BCAL energy versus FCAL energy for events with at least one hit in the start counter for electromagnetic background (left), hadronic background (middle), and signal events (right). The solid curve represents the threshold applied in the analysis.

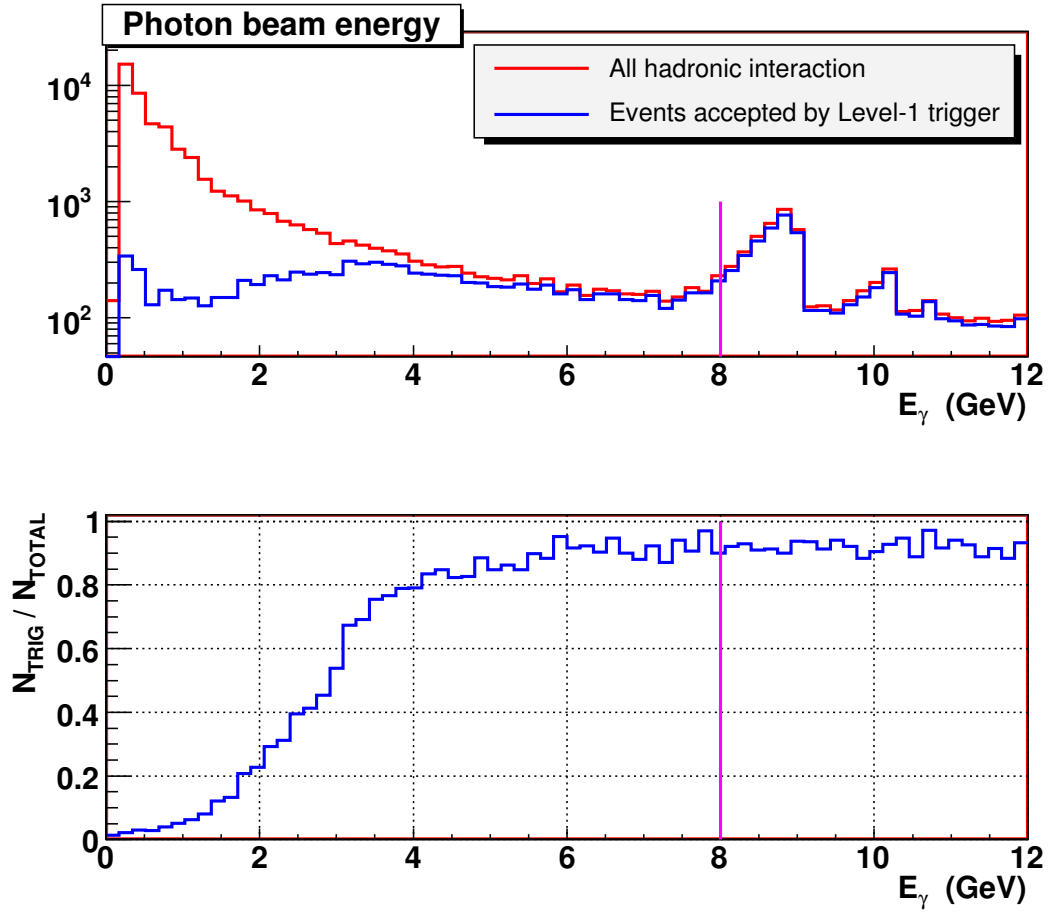


Figure 9: Energy spectra of beam photons for all events produced in hadronic interactions and those accepted by the Level-1 trigger (top). The trigger acceptance as function of the beam energy (bottom).

5 Conclusion

We have completed a simulation of the Level-1 trigger system, which show that we achieved our goals. The simulation inputs and results are as follows:

- Realistic simulation of hadronic interactions using PYTHIA with $E_\gamma > 3$ GeV and empirical representation of total cross section for $E_\gamma < 3$ GeV.
- Realistic simulation of electromagnetic interactions incorporating all material of the detector into the geometry.
- Generation of hits in the detector with realistic thresholds.
- Simple algorithm for the Level-1 trigger predicts a Level-1 rate of 150 kHz and efficiency for signal of about 93%.
- Algorithm is effective at eliminating electromagnetic background and hadronic interactions below 4 GeV.

References

- [1] A. Biselli et al. A search for QCD exotics using a beam of photons, 2002. Proposal. [3](#)
- [2] W. M. Yao et al. Review of particle physics. *J. Phys.*, G33:1–1232, 2006. [3](#)
- [3] Torbjorn Sjostrand, Leif Lonnblad, and Stephen Mrenna. PYTHIA 6.2: Physics and manual. 2001. [6](#)
- [4] A. Dzierba. Comparing PYTHIA simulation with photoproduction data at 9 GeV. GlueX document server, 2007. URL <http://portal.gluex.org/>. GlueX-doc-856. [6](#)
- [5] S. S. Kamalov et al. Dispersion relation analysis of neutral pion photo- and electroproduction at threshold using the MAID and SAID solutions. *Phys. Rev.*, C66:065206, 2002. [6](#)
- [6] A. Baldini, V. Flaminio, W. G. Moorhead, Douglas R. O. Morrison, and (Ed.) Schopper, H. Total cross-sections for reactions of high-energy particles. Berlin, Germany: Springer (1988) 409 p. (Landolt-Boernstein. new series, 1/12B). [8](#)
- [7] HEPDATA: Reaction Database. URL <http://www.slac.stanford.edu/spires/hepdata/>. [8](#)
- [8] R. Brun et al. GEANT Detector Description and Simulation Tool, CERN Program Library (1993). We use GEANT version 3.21. [10](#)
- [9] GlueX collaboration. GlueX/Hall D Calorimeter Final Design and Safety Review. February 19-20,2008. [10](#)